The Thesis committee for Garrett Morgan Salpeter

Certifies that this is the approved version of the following thesis:

Optimization of Material Composition and Processing Parameters for Hybrid Organic-Inorganic Solar Cells

APPROVED BY

SUPERVISING COMMITTEE:

Supervisor: _____

Arumugam Manthiram

_____

Paulo Ferreira

Optimization of Material Composition and Processing Parameters for Hybrid Organic-Inorganic Solar Cells

by

Garrett Morgan Salpeter, B.A.

Thesis

Presented to the Faculty of the Graduate School

of the University of Texas at Austin

in Partial Fulfillment

of the Requirements

for the Degree of

Master of Science in Engineering

The University of Texas at Austin

December, 2010

Acknowledgements

I am forever grateful to my family, particularly my father, mother, and sister for the inspiration to pursue that which is important to me. I am deeply indebted to Professor Arumugam Manthiram for his guidance, and especially for the patience and grace with which he helped me navigate my experience in graduate school. I am also thankful for Dr. Paulo Ferreira for volunteering to serve on my Thesis committee.

This particular project was not possible without the assistance of several colleagues. Reeja Jayan helped me learn many techniques that I needed in the lab and also instructed me in the use of several different pieces of equipment. Along with Dr. Jim Ciulik, she also revived an old evaporator, using spare parts and a large amount of ingenuity. Nick Folse's programming ability was apparent with every cell I tested. The LabView program that he created for our testing setup was seamlessly integrated and easy to use. I am also grateful to Chelsea Lawson for her assistance working with the metal shop team to create the mask and holders that we needed during the course of our cell processing.

December, 2010

Abstract

Optimization of Material Composition and Processing Parameters for Hybrid Organic-Inorganic Solar Cells

by

Garrett Morgan Salpeter, MSE

The University of Texas at Austin, 2010

SUPERVISOR: Arumugam Manthiram

The widespread adoption of hybrid organic-inorganic solar cells has been delayed by low performance. Improving performance requires a firm understanding of how to optimize both material composition and processing parameters. In this thesis, we examine processing parameters that include solution composition, annealing temperature, and the rates of spin casting and evaporative coating. We also find that the optimal weight ratio for the active layer of a ZnO:P3HT solar cell is 40 wt. % ZnO.

TABLE OF CONTENTS

CHAPTER 1

INTRODUCTION

The United States Energy Information Administration (EIA)[1] recently released its 2010 *International Energy Outlook (IEO).* In this report, they forecast that the world's energy consumption will rise by 49 percent from 2007 to 2035 and question the viability of coal and petroleum-based fuel sources in light of issues with supply and legislation. As a natural consequence, the EIA expects the amount of energy generated by renewable sources to grow, and also points out the large amount of work that must be done to develop renewable sources of energy and fill the gap that they see developing.

Because the sun provides renewable energy to our planet in an amount that can meet the world's energy demand many times over, photovoltaics (PV) become an attractive approach to help meet the world's growing energy demands [2-4]. Relative to the conventional sources of energy like oil, coal, natural gas, and nuclear, photovoltaics also provides useable energy that is less harmful to the environment and more consistently available and geographically versatile, and from a local American perspective, a boost to national security

[5]. Currently, only 0.1 % of the total electricity generated in the United States comes directly from sunlight [4].

In the year 2005, more than 90 % of the photovoltaic cells manufactured around the world were made with crystalline silicon (c-Si). Virtually all of the rest were made with thin-film technologies like amorphous silicon (a-Si), cadmium-indium-gallium-selenide (CIGS), and cadmium telluride (CdTe) [6]. Though the roadmaps of the energy administrations of the United Nations, United States, and European Union call for Si technology to remain the most popular for at least the next 20 years, they all forecast that new technologies like dye-sensitized solar cells and organic solar cells will see an increased market share. It is also a stunning statistic, and a probable sign of things to come, that since 1990, 27 % of worldwide patent applications have been related to organic solar cells [7].

1.1 Organic solar cells

Organic materials for photovoltaics are particularly attractive because they are less expensive, more readily available, and can be processed in solution. These factors can bring the total manufacturing cost down compared

to traditional silicon cells or other thin-film cells like CIGS. But even with the lower cost of manufacturing, these organic cells still need to perform better in order to compete with traditional methods of power generation.

The foundation for the field of organic photovoltaics was laid by Heeger, MacDiarmid, and Shirakawa, who discovered conductive polymers in the late 1970's [8]. This discovery earned them the 2000 Nobel Prize in Chemistry. In 1995, Heeger's group at UC-Santa Barbara published a landmark study using a blend of the polymer poly(2-methoxy-5-(2`-ethyl-hexyloxy)-1,4-phenylene vinylene) (MEH-PPV) with phenyl-C_{61}-butyric acid methyl ester (PCBM) to make a working photovoltaic device [9]. This work established the conjugated polymer-based model of organic photovoltaics, and this material combination currently provides the best performing organic solar cell, having reached a power conversion efficiency of 6 % [10].

1.2 Organic polymers

Recent developments of additional conductive polymers have also added to the variety of types of organic solar cells. The most versatile and widely studied polymers in electronics, polythiophenes, are easily synthesized and

modified and are the best performing polymers. They are also soluble in a variety of organic solvents due to irregular functional groups. This structure, however, also leads to steric interactions, which limit conformation and can alter the polymer's energy levels [10]. Even still, polythiophenes are strong absorbers across a broad range of energies. Their energy gap matches the energies of photons in the visible spectrum; additionally, they can also absorb lower energy photons because of domains with extended π-stacking, which supports intermolecular excitons [11].

Shown in Fig. 1, P3HT, which is poly(3-hexylthiophene-2,5-diyl) [12] is particularly attractive because of its high hole mobility. It is also soluble in a variety of organic solvents, and tends to crystallize into ordered domains [13]. Because of these qualities, P3HT in particular is being very heavily studied among the polythiophenes in many types of organic electronics.

1.3 Hybrid organic-inorganic photovoltaics

In recent years, attempts have been made to use inorganic materials to replace PCBM alongside the polymer in organic solar cells. In addition to being less expensive than PCBM, these inorganic materials often have energy levels

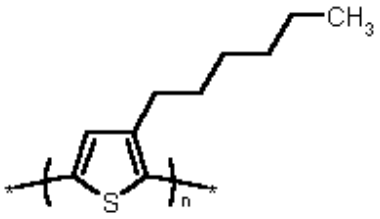

Figure 1. Structure of Poly(3-hexylthiophene-2,5-diyl) used in this thesis. Image from Rieke Materials catalog [12].

that align better with the electron donors like P3HT. For example, the difference between the LUMO levels of P3HT and PCBM is more than 500 mV higher than it needs to be for electron transfer to occur [4]. This 500 mV is lost, a casualty of selecting a non-ideal material. Inorganic electron acceptors that have been used include ZnO [14-16], CdSe [17], TiO_2 [18], PbSe [19], $CuInS_2$ [20], as well as CuPc [21-23] and ZnPc [24] combined with C_{60} fullerene molecules.

Titanium dioxide in particular has gotten a lot of attention because of its extensive use in dye-sensitized solar cells. Greenham [25] mentions that metal oxides like TiO_2 offer advantages such as being less toxic than most II-VI semiconductors, relatively easy to synthesize, less expensive, and electronically conductive. They also have higher dielectric constants than organic materials, meaning that they absorb a larger portion of the energy in an incident electric

field. This quality makes for a lower exciton binding energy, the importance of which is discussed in the following section.

1.3.1 Zinc oxide:P3HT solar cells

Zinc oxide (ZnO) is an attractive material for many of the same reasons as TiO_2, plus its energy bands are naturally positioned to accept electrons from P3HT by allowing exciton dissociation with minimal energy loss. As shown in Fig. 2, it is incorporated into the active layer of the cells used in this thesis.

1.3.2 Device performance and architecture

Photons in hybrid organic-inorganic cells are absorbed by the polymer, creating an exciton. Unlike the free electron and hole created upon absorption in a typical semiconductor, this exciton is a bound electron-hole pair in an excited state. Though the exciton is created, Fig. 3(a) shows that the energy levels in organic semiconductors are analogous to those in inorganic

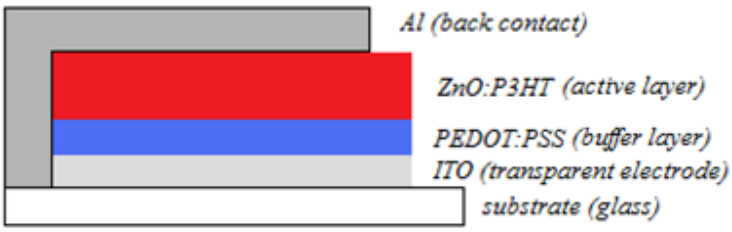

Figure 2. Schematic of P3HT:ZnO solar cell architecture and (b) bulk heterojunction morphology.

semiconductors. To be converted to free charge carriers, this exciton must move to a donor-acceptor interface where it will dissociate. This dissociation process takes further energy, which must be supplied by the electric field of the device. Upon dissociation, the electron will transfer to the inorganic acceptor, and the hole will recede back into the polymer. This whole process is guided by the energy levels of Fig. 3(b) [31-34].

If an exciton does not reach a donor-acceptor interface before it recombines, the energy is of the exciton is lost as waste heat and cannot be used. When the electron recombines with the same hole with which it was originally generated, this recombination is known as geminate recombination. Geminate recombination is, in fact, the dominant factor in quantum efficiency

(conversion of absorbed photon to free charge carrier) and current-voltage performance [26]. It is, therefore, of critical importance that excitons are created in close enough proximity to an interface so that they can diffuse and be separated before recombination. In P3HT, the typical exciton diffusion length is only 5 - 10 nm [27]. This short length necessitates intimate contact between P3HT and ZnO domains, and is the motivation for the bulk heterojunction architecture.

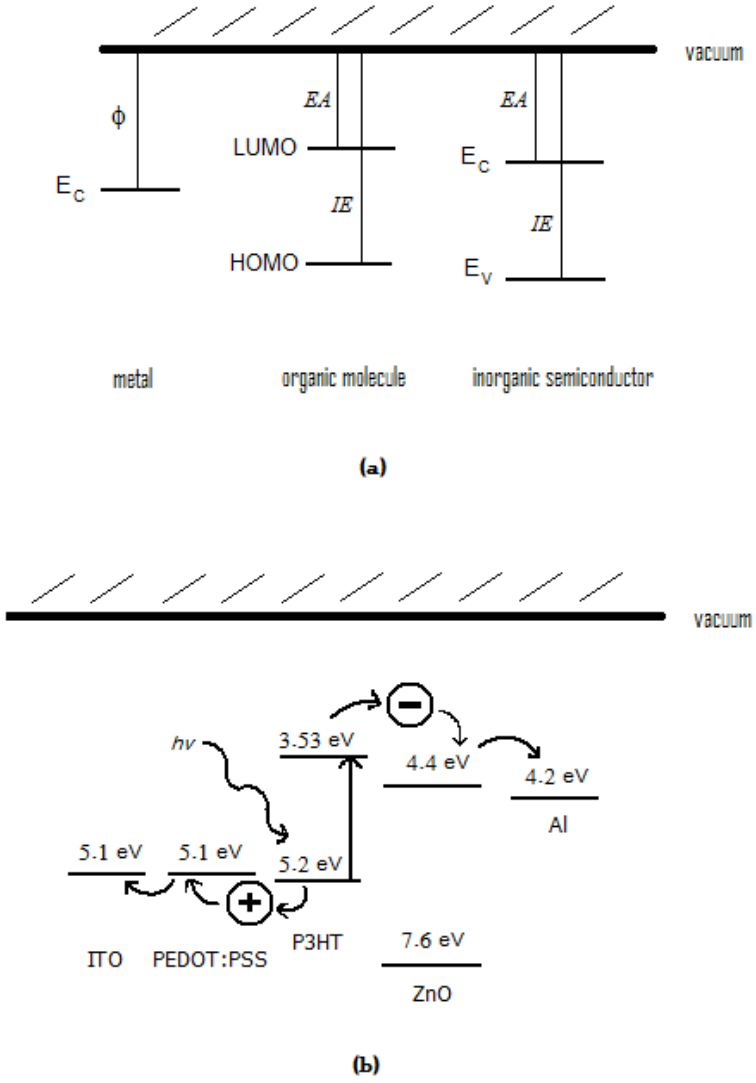

Figure 3. (a) Relevant energy levels in metals and organic/inorganic semiconductors and (b) the energy schematic of a ZnO:P3HT solar cell with the relevant energy levels (the values are from refs. 31-34). It is observed that the LUMO in organics is analogous to the conduction band in inorganics; similarly, the HOMO is analogous to the valence band. ϕ is the work function, or energy required to strip an electron from a metal. IE is the ionization energy, or energy required to strip an electron from a nonmetal, and EA is the electron affinity, or energy given off when a material accepts an electron.

As shown in Fig. 4, a bulk heterojunction is a somewhat random mixture of two different components that must have two features to work successfully. First, the two components must be very intimately mixed. That is to say the interfacial area between the two phases should be maximized. It is also important that every exciton generated in P3HT is within that 5-10 nm diffusion length of a ZnO domain. Second, from every interface, each of the phases must form a continuous path to its respective electrode so that there can be a net positive current to an external load. Due to the kinetics of bulk heterojunction ordering, altering the film casting conditions can tailor the degree of crystallization and the zinc oxide – P3HT phase separation [4].

Figure 4. Bulk heterojunction: the red region corresponds to P3HT, while the yellow region corresponds to ZnO. Only the ZnO domains that connect to the top contact are useful for charge transfer, as the isolated domains cannot provide a path for electrons to reach the external circuit.

Since the charge separation occurs at the interface, the open-circuit voltage (V_{oc}) evolves from the energy gradient at this point. Specifically, it depends on the offset between the HOMO level of the P3HT and the LUMO of ZnO. Shown in Fig. 3(b), these energy levels provide a maximum open-circuit voltage of 0.8 V.

Short circuit current (J_{sc}) depends on the efficiency of charge separation. It is, therefore, a product of the very structure itself. To have current that can power an external load, two things need to happen with an exciton. First, it must reach an interface to dissociate. This is where the intimate mixing of the bulk heterojunction structure comes in. As mentioned above, these excitons need additional energy to dissociate; that additional energy is found in the band offsets at the donor-acceptor interface. Second, the unbound electron must have a ZnO path that carries it all the way to the cathode (back contact), while the unbound hole must have a P3HT path that leads all the way to the anode (transparent electrode) of Fig. 2. Hopping of electrons between ZnO nanoparticles is, therefore, a major factor in device operation [25].

The other primary parameter measuring solar cell performance is fill factor. As a measure of the shape of the current-voltage curve, fill factor

depends strongly on carrier recombination strength, buildup of space charge, and shunt and series resistances [10]. These factors are all significantly affected by the structure and the integrity of the charge transfer paths in the active layer.

Work done on MDMO-PPV:ZnO cells demonstrates that the ratio of the materials used has a profound impact on performance [28]. In fact, this ratio appears to be one of the most important variables that must be optimized to raise device efficiency. We expected the P3HT:ZnO ratio to have a similarly vital effect in this type of cell, and the investigations reported later in this paper prove that supposition to be true.

1.4 PEDOT:PSS buffer layer and aluminum and indium tin oxide electrodes

Poly(2,4-alkylenedioxythiophenes), or PEDOT type polymers, are used as a buffer layer in ZnO:P3HT solar cells. As shown in Fig. 2, this layer is sandwiched between the active layer and the transparent indium tin oxide anode. Combined with polystyrene sulfonic acid to make PEDOT:PSS, this material has a low HOMO-LUMO band gap that allows for a tremendously

stable, intrinsically conductive polymer that is a material of choice for organic light-emitting diodes and organic solar cells [29].

PEDOT:PSS is usually in an aqueous dispersion, and is most reliably deposited by spin coating. Once deposited, these films should be annealed to remove water content in most devices. The material will also take up moisture when handled in ambient after baking, so processing in an inert atmosphere is important for achieving reproducible results [30].

The major benefit of incorporating PEDOT:PSS into these solar cells is that it helps to planarize the rough indium tin oxide surface. In fact, according to Jonda *et. al.* [35], a 50 nm layer of PEDOT:PSS can reduce the root-mean-square roughness of ITO from 10 nm to 3 nm. This increased smoothness can have dramatic, positive ramifications for the conversion efficiency of this device by decreasing the instance of electrical shorts [30].

With the energy profile of Fig. 3(b), PEDOT:PSS is a seamless step in the transport of holes to the transparent electrode. More importantly, it also diminishes the importance of the ITO work function because it has such a high density of free charge carriers that the Fermi levels of ITO and PEDOT:PSS

become continuous as in perfect metals. Also, the mobility is high enough that the voltage drop across this buffer layer can be neglected [36].

There are two problems with PEDOT:PSS that warrant attention. The first is that it is acidic, with a pH in the range of 1 – 2. Such acidity is suspected to dissolve indium from the ITO electrode, which can then potentially migrate to the active layer. Such impurities degrade the performance of the device [37]. The second is that, as mentioned before, PEDOT:PSS takes up water. If this water gets into the device, it can corrode metal contacts or damage other organic semiconductors. Processing in an inert atmosphere is the best way to alleviate this problem.

The aluminum and indium-tin-oxide (ITO) electrodes of Figs. 2 and 3(b) are the final materials required to maximize this cell performance. Al is a metal with a work function ϕ,of -4.2 eV; this aligns just beneath the LUMO of ZnO to allow seamless transport of electrons to the external circuit with minimal energy loss. The opposite contact must be transparent, because the photons from sunlight must pass through this layer to get to the active layer and be absorbed. ITO is a transparent, conductive oxide with ϕ = -5.1 eV.

1.5 Solution processing

As mentioned above, the ability of these materials to be processed in solution has the potential to make large-scale production of hybrid organic-inorganic cells much less expensive than the existing PV technology. It can even enable the possibility of roll-to-roll processing. The first major variable when discussing solutions is which solvent to choose. The active layer must be spin cast from a solution, in which the solvent must be able to dissolve both the organic P3HT and the inorganic ZnO. Solubility of P3HT increases in switching from methanol to hexane, increases again moving on going to xylene, and reaches a maximum with chloroform [38]. Fortunately, chloroform is a common organic in which ZnO also has a high enough level of solubility to prepare the active layer [28].

When dealing with films cast from solution, it is known that slower drying of films allows reorganization, which yields three dimensional crystalline order [39-40]. Faster deposition, as in spin casting, alters the molecular orientation; if too fast, it prevents significant reorganization and results in a material with many agglomerates [41]. Spin rate, therefore, is a very important parameter in cell-making, since it affects the rate at which the solvent dissolves

– and, ultimately the morphology. Factors that still need to be understood include differential solubilities of polymers and nanocrystals, nanocrystal aggregation in solution, instabilities during spin coating, and differential evaporation from solution [42].

1.6 Objectives of this thesis

To compete with existing photovoltaic technologies, these ZnO:P3HT cells must perform at much higher levels than they are currently able to achieve. That performance depends intimately on cell processing and material composition. Accordingly, the purpose of this thesis is to observe how material composition and processing parameters affect the performance of these ZnO:P3HT solar cells, and then to use that information to optimize the cells. In particular, the material composition to be optimized includes the concentration of materials processed in solution as well as the ratio of ZnO and P3HT in the active layer. Processing parameters to be optimized include spin coating and material deposition rates, annealing temperatures, and methods of ZnO nanoparticle synthesis.

CHAPTER 2

EXPERIMENTAL METHODS

A portion of this work focused on optimizing processing conditions for P3HT:ZnO solar cells. The materials making up the cells are important, but the same materials can perform in widely varying ways depending on how they are processed.

2.1 Substrate preparation

The ITO-on-glass slides (commercially available from Nanocs) were etched to decrease the area covered by ITO so that the back contact could be added to the solar cell. The slides were covered with Kapton (polyimide) tape, leaving exposed the ITO that was to be removed with etchant. On average, resistance across the ITO surface was approximately 20 Ω to begin with. The etchant solution consisted of 2 mL nitric acid and 5 mL hydrochloric acid added to 13 mL deionized water. This solution was heated to 75 ^{o}C, and the glass slide was added to the solution for five minutes. The glass slide was then moved to a beaker of tap water to rinse off any remaining etchant, and the Kapton tape

was removed. Finally, the etching was verified with resistance measurements showing that the area that was etched had immeasurably high resistance, while the non-etched area demonstrated 25-30 Ω resistance across the length of the surface.

After etching, the slides were then cleaned by sonication in a series of solutions [43-44]. Each sonication step was 10 minutes in duration. First, the slides were placed in beakers with ~15-20 mL solution of Alconox detergent (pre-mixed with deionized water) and sonicated. Next, sonication was done in the same amount of deionized water, the slides were rinsed, and the step was repeated once more with deionized water. The slides were then successively sonicated in solvents of acetone and isopropyl alcohol. Finally, they were cleaned using a Harrick PDC-32G plasma cleaner. The plasma cleaner was used with O_2, and ran for three minutes on the unit's "medium" setting.

2.2 Zinc oxide nanoparticle synthesis

Among other variables, this thesis compared the effect of ZnO particle size on cell performance. To that end, two primary sizes were used. The first was a commercially available ZnO powder (Alfa Aesar, Zinc oxide NanoGard®)

with a nominal particle diameter of 100 nm. The x-ray diffraction data for this powder is shown in Fig. 5(a). The second was a ZnO nanoparticle prepared by solution processing specifically in this thesis.

These ZnO nanoparticles were made using a combination of methods from available in the literature [28,45,46]. This hybrid method used two precursor solutions. The first was 2.95 g zinc acetate dihydrate (98+%, commercially available from Acros Organics) dissolved in 125 mL methanol (Fisher Scientific). This solution was heated to 60 ^{o}C.

The second solution contained 1.48 g potassium hydroxide (Fisher Scientific) dissolved in 65 mL methanol. Under vigorous stirring, this second solution was added to the first over a period of thirty minutes using a burette. The resulting solution was heated and stirred for four hours. It was then put in a centrifuge for thirty minutes to separate the precipitate and mother liquid, washed once with 40 mL of methanol, and allowed to rest for one hour. Finally, the solution was run through the centrifuge one more time, the mother liquid was poured off, and the precipitated nanoparticles were treated with 10 mL of chloroform (Fisher Scientific). This final solution was mixed with P3HT to form the bulk heterojunction for the active layer of the nanoparticle cells. Based on

XRD data, it was observed that the structural integrity of the nanoparticles in solution remained for one week; the particles could not be used if they were kept in solution for more than a week.

The resulting nanoparticles were examined by X-ray diffraction, and the results are shown in Fig. 5(b). The additional peaks at $2\theta = 50^{o}$ and 60^{o} indicate the presence of some zinc hydroxide in addition to the zinc oxide. The X-ray diffraction results were taken using a Philips APD 3520 powder diffractometer in the range of $2\theta = 25\text{-}80°$, with 0.01° steps and a five second dwell time. The results of the XRD were used to determine the size of the nanoparticles using the Debye-Scherrer equation [47],

$$d = 0.9\lambda/(B\cos\theta),$$

where d is the average diameter of the particle, λ is the wavelength of the radiation used, B is the FWHM in radians, and θ is half of the scattering angle. These calculations show that the diameter of the nanoparticles was approximately 8-10 nm. These calculations used the four most intense peaks, averaging them together. Similar calculations confirmed that the commercially available 100 nm diameter ZnO particles were 100 nm in diameter.

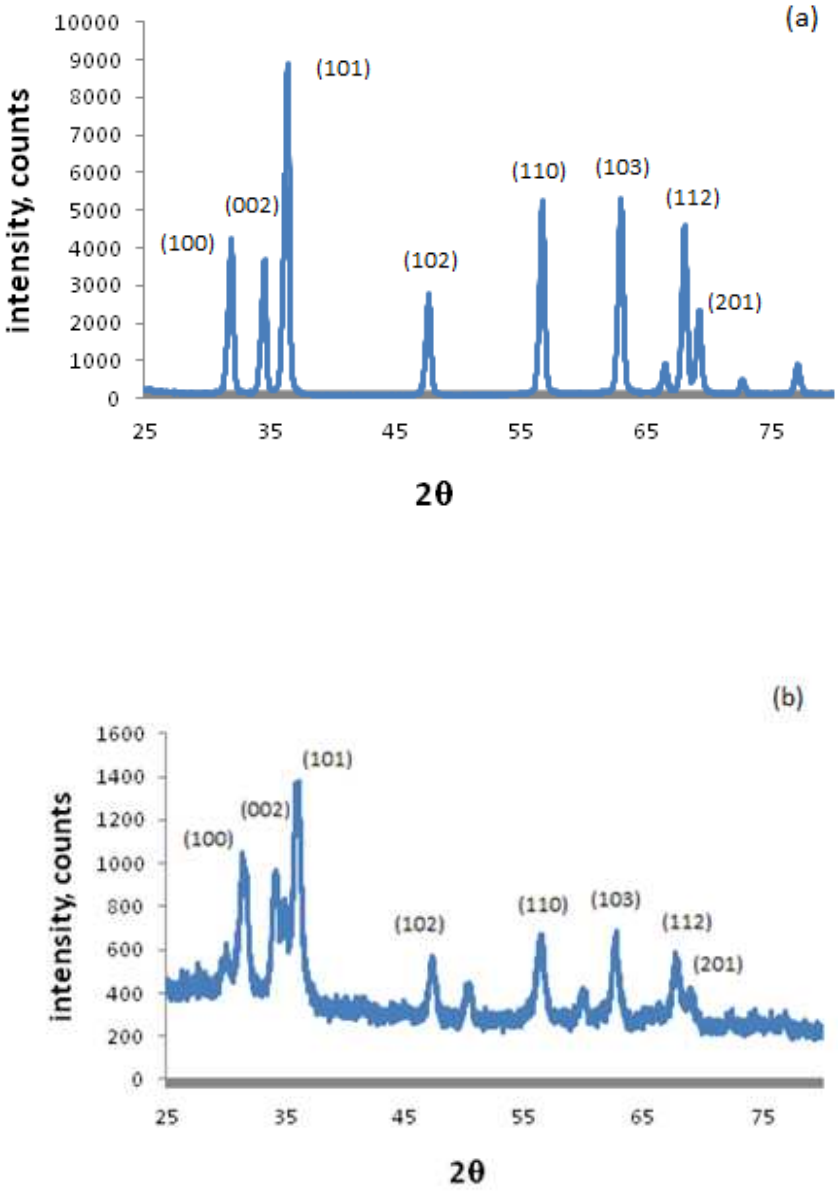

Figure 5. X-ray diffraction pattern of ZnO nanoparticles used in the active layer of solar cells. (a) The commercially available 100 nm diameter particles demonstrate a pattern with less noise than the (b) solution processed, 10 nm diameter particles. FWHM calculations confirm the particle sizes.

2.3 Mixing with P3HT

The P3HT (Rieke Materials) was weighed and mixed with chloroform in a sealed, amber vial and stirred for five hours on a hot plate (Torrey Pines Scientific) at 900 rpm and 50 °C in an argon atmosphere. An appropriate amount of ZnO nanoparticle solution was mixed this P3HT solution to achieve the desired material ratio, and the combination was stirred at 900 rpm and 50 °C for 24 hours in an argon atmosphere.

2.4 Depositing

PEDOT:PSS (H.C. Starck, Inc.) was spin coated using a KW-4A Spin Coater from Chemat Technologies, followed by a transfer to the hot plate for annealing to remove the excess water. After annealing, the bulk heterojunction layer was spin coated. The spin rates are discussed in the next section.

2.5 Aluminum evaporation

For evaporation of the aluminum electrode, the cells were placed in the mask shown in Fig. 6(a) so that the electrodes would be the correct size and

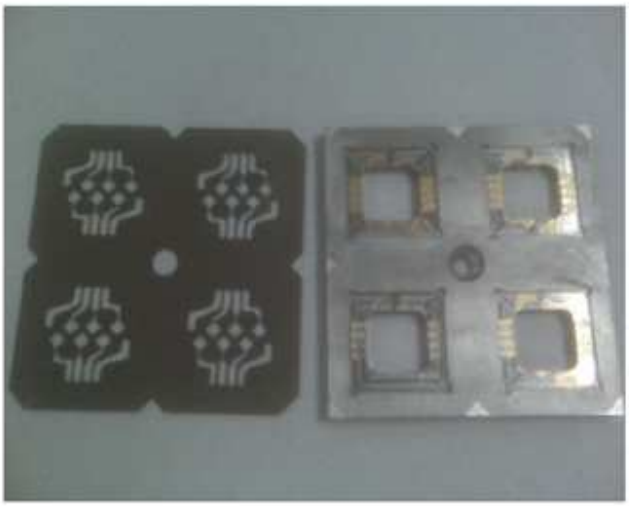

(a)

(b)

Figure 6. (a) The mask used for aluminum deposition and (b) the evaporator used for aluminum deposition.

shape. The electrode was coated using an old evaporator shown in Fig. 6(b) that was reconfigured with spare parts. Unfortunately, in transferring the cells to the evaporator, they had to be brought out of the glove box and exposed to air. The operating parameters are discussed in Chapter 3.

2.6 Annealing

The first annealing step was already mentioned; it took place immediately after the PEDOT:PSS is deposited to remove the excess water. The final annealing step took place after the aluminum electrode was deposited. Annealing was performed in an argon atmosphere for ten minutes at various temperatures, the effects of which are described in the results section. The finished cell is shown in Fig 7.

2.7 Testing

Testing was performed in a special set-up described below. The cells were placed in a mount with connections to a Keithley 2400 electronic multimeter that measured both current and voltage. The mount was in the

(a)

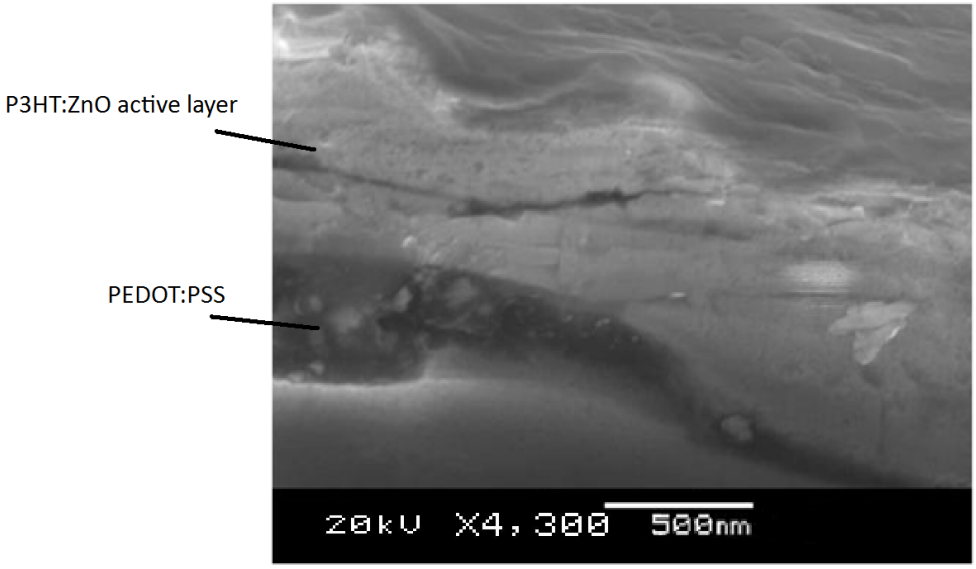

(b)

Figure 7. (a) An example of a finished cell and (b) SEM image (taken with a JEOL JSM-5600) of a P3HT:ZnO solar cell made in this thesis.

same argon atmosphere as all previous steps, with the exception of aluminum evaporation. They were illuminated by an AM 1.5 solar simulator (Newport), and the current-voltage data was read into a custom LabView program.

One consideration that has to be taken into account when testing is that short-circuit current density calculations use the area of aluminum cathode [43]. The area of this contact, controlled by the mask used during deposition, is 0.09 cm^2. Also, since thermal stress and visible light soaking erode the stability of the cells due to morphological changes and photochemical polymer degradation, the light source was only illuminating the cells for one second at a time while performance measurements were taken [48].

CHAPTER 3

RESULTS AND DISCUSSION

As mentioned above, much of this work deals with optimizing processing conditions to maximize the performance of the materials used. Several variables regarding the material composition were also studied, and this section presents the results of attempts to optimize both processing conditions and materials composition.

3.1 Aluminum deposition

To figure out how to appropriately use the evaporator to deposit the correct amount of aluminum for the back contact, experiments were undertaken to determine the rate at which aluminum was deposited. It is important that one not deposit too rapidly, or else the high energy aluminum particles can ablate other particles from the surface. At the same time, the current must be high enough to vaporize the aluminum. Therefore, the optimal level is the lowest temperature that causes vaporization.

The evaporator is configured with aluminum wire wound into a tight ball and heated to evaporation in a tungsten wire basket. The two variables involved were amount of time and amount of current used in the heating element. The minimum level of current that we could monitor with this apparatus is 10 A, so that was chosen as the starting point. At this level of current, the basket did not heat up enough to vaporize the aluminum. With increasing the current, appropriate vaporization was observed at approximately 15 A, and that level of current was chosen.

The time was then varied to determine the duration required to reach a thickness of 100 nm, which had been shown in the literature to be an acceptable number [15]. Measurements taken with the Veeco Dektak3 surface profiler demonstrate that evaporation at 15 A for two minutes yielded an approximate thickness of 40 nm, five minutes yielded 70 nm, and seven minutes yielded 100 nm. Thus, seven minutes was chosen.

3.2 PEDOT:PSS and active layer deposition

Similarly, the surface profiler was used to help determine optimal settings for the deposition of solutions with the use of the spin coater. As had

been documented in the literature, we wanted to achieve a PEDOT:PSS layer thickness of approximately 50 nm, and an active layer thickness in the range of ca. 250 - 300 nm [14,25].

With spin coating, it is difficult to get even coverage of the substrate because different parts of the substrate move at different velocities as the glass slide spins. Measurements were taken on the relevant area of the surface (the part at which the aluminum contacts were deposited) so that the thicknesses would be as accurate as possible.

With the other variables of operation, we opted for the equipment's default parameters. These parameters included starting with 10 s of rotation at 500 rpm, followed by 60 s of rotation at the speed we chose. With PEDOT:PSS, 60 s of rotation at 2000 rpm yielded a layer thickness of approximately 90 nm, while rotation at 3000 rpm yielded the desired layer thickness of approximately 50 nm.

With the standard active layer solution, we again started with 2000 rpm. This speed yielded an active layer thickness of approximately 200 nm, while 1750 rpm yielded an approximate layer thickness of 240 nm, and 1500 rpm (the

minimum spin rate) yielded an approximate layer thickness of 270 nm. Thus, 1500 rpm was chosen.

3.3 Annealing temperature

In optimizing the production process, one of the most important variables is the temperature at which the cells are annealed. In only one paper referring to similar cells is an annealing temperature specifically mentioned, and that temperature is 160 ^{o}C [49]. Since the annealing done in that particular setup was in a vacuum oven rather than a hot plate, a slightly lower temperature range was first examined.

As shown in Fig. 8, cells were annealed at temperatures of 90 ^{o}C, 110 ^{o}C, 130 ^{o}C, and 150 ^{o}C. Short circuit current density increased with increasing temperature to 130 ^{o}C, then decreased again at 150 ^{o}C. Open circuit voltage actually decreased with increasing annealing temperature throughout the range tested. Most importantly, the overall performance measured by output power followed the trend of the short circuit current, increasing with increasing temperature up to 130 ^{o}C, where it peaked and then decreased again at 150 ^{o}C.

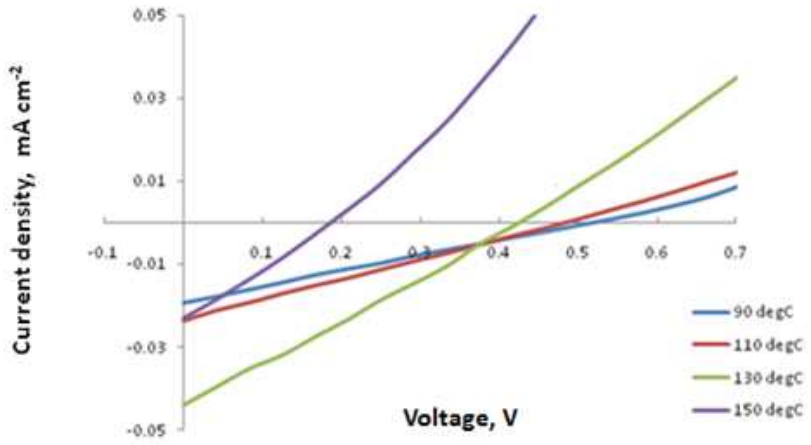

Figure 8. J-V performance of cells processed with identical materials and through identical steps, with the exception of the temperature of the annealing steps after deposition of the PEDOT:PSS layer and the Al contact.

3.4 Active layer solution concentration

The cells to be made in the architecture of Figure 2(a) are to match the P3HT:ZnO cells that had performed best in the literature [15]. Deferring to the literature on the order and thickness of layers, the major remaining variables that affect performance are those related to material composition of the active layer. The first step in determining the appropriate material composition is to

find the optimal concentration for the solutions from which the active layer is deposited.

This comparison was first attempted with the smaller 10 nm ZnO particles. The most frequent examples in the literature were 20 and 10 mgmL^{-1}. In all, concentrations of 5, 10, 15, and 20 mg mL^{-1} were chosen for testing. As shown in Table 1, cells made with solution concentrations of 10 mg mL^{-1} exhibited the best performance at both ratios of P3HT and ZnO.

Therefore, all further cells were made with active layers deposited from solutions with a material concentration of 10 mg mL^{-1}. The next variable to be tested was the size of the ZnO nanoparticles. In the examples given in the literature, great care and extra effort were taken to synthesize nanoparticles on the order of 1-10 nm. If larger, less expensive, and more easily synthesized particles could be used with no loss in performance, then that substitution would be a step towards the goal of bringing down the cost of these cells.

Table 1: Cell performance varying with material composition and solution concentration for cells with 10 nm ZnO particles in the active layer. The best performing cells are in bold (based on power output).

Wt. % ZnO	concentration (mg mL^{-1})	V_{oc} (V)	J_{sc} (mA cm^{-2})	FF	Power (mW cm^{-2})
50	20	0.07	0.46	0.25	0.008
50	15	0.08	0.63	0.27	0.014
50	**10**	**0.08**	**0.72**	**0.28**	**0.016**
50	5	0.07	0.59	0.28	0.012
40	20	0.17	0.40	0.26	0.018
40	15	0.17	0.57	0.28	0.027
40	**10**	**0.17**	**0.62**	**0.28**	**0.030**
40	5	0.16	0.54	0.28	0.024

3.5 Size of ZnO nanoparticles

For ZnO nanoparticles to be made on the order of 1-10 nm in diameter, many effort-intensive processes must be carried out. 100 nm ZnO particles, on the other hand, are commercially available and much less expensive than the cost of the solvents and precursors used in all of the nanoparticle synthesis methods reviewed for the work in this thesis. No studies have shown either if such large particles could function in P3HT:ZnO solar cells, or to what degree they affect the performance of these cells. Such observations should help gain further insight into the morphology of these cells and how it affects performance.

As shown in Table 2, the cells made with the 100 nm ZnO particles were significantly outperformed by those made with the 10 nm ZnO particles at all three material ratios tested. Two primary effects were noted to explain this general observation. First, the voltage was actually higher for the cells made with larger ZnO particles. Since voltage depends on the energy level splitting between donor and acceptor, the larger ZnO particles probably preserve the integrity of the P3HT domains and structure, creating more P3HT-P3HT interactions and maintaining the energy levels. This is most likely due to larger

amounts of agglomeration and phase segregation. Second, the current increased by a factor of 20-40 with the smaller ZnO particles. Since the ability of the cell to transfer charge is intimately related to exciton dissociation and percolation pathways in the active layer, the smaller particles must allow for a more intimate mixing of materials and a better connection of ZnO particles to form such pathways.

Table 2: Variation of cell performance with composition and size of ZnO particles in the active layer.

Wt. % ZnO	Diameter of ZnO particles (nm)	V_{oc} (V)	J_{sc} (mA cm^{-2})	FF	Power (mW cm^{-2})
60	100	0.20	0.042	0.25	0.0021
60	10	0.08	0.78	0.26	0.016
50	100	0.27	0.026	0.27	0.0019
50	10	0.08	0.72	0.28	0.016
40	100	0.44	0.021	0.24	0.0022
40	10	0.17	0.622	0.28	0.0296

3.6 Cell material composition

Examples in the literature have mentioned an optimal material composition for the P3HT:ZnO cell, but none has given a quantitative analysis of how that composition was determined or the effect of varying composition on cell performance. Such a quantitative analysis was a major goal of this project.

Many works in the literature found optimal performance at a P3HT:ZnO ratio of 50 wt. % : 50 wt. % [14,15,50]. As shown in Table 3 and Fig. 9, this tested ratios in this thesis included ZnO compositions of 30, 35, 40, 45, 50, and 60 wt. %. These values were chosen by starting with the 50 wt. % value that other groups had found, and then 40 and 60 wt. % were arbitrarily chosen to observe how altering the amount of ZnO affects the performance. It was seen that performance improved by lowering the amount of ZnO to 40 wt. % and became worse by increasing the amount of ZnO to 60 wt. %. Therefore, the next steps required looking at other amounts of ZnO in the direction that improved performance until the optimal amount was found.

It turned out that 40 wt. % was the optimal amount, as both increasing or decreasing the ZnO from that point reduced the overall power output of the cell. As shown in Fig. 10, this cell achieved V_{oc} = 0.17 V, J_{sc} = 0.62 V, FF = 0.28,

and overall power conversion efficiency, η = 0.03%. These results are in slight contrast to those of Beek [15] and Oosterhout [50], which optimized performance with 50 wt. % ZnO. These studies used cells with thinner active layers (about 50-100 nm thinner), limiting the number of photons that could be absorbed.

Table 3: Variation of cell performance with composition for cells with 10 nm ZnO particles in the active layer.

Wt. % ZnO	V_{oc} (V)	J_{sc} (mA cm^{-2})	FF	Power (mW cm^{-2})
60	0.08	0.78	0.26	0.016
50	0.08	0.72	0.28	0.016
45	0.12	0.68	0.27	0.022
40	0.17	0.62	0.28	0.030
35	0.28	0.31	0.26	0.023
30	0.35	0.14	0.25	0.013

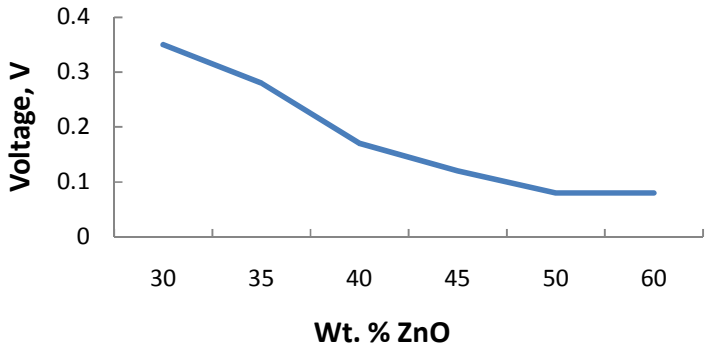

(a)

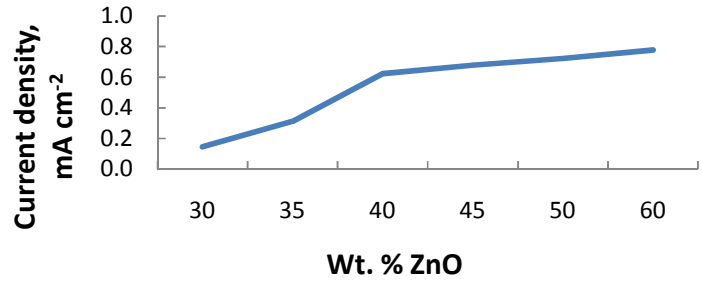

(b)

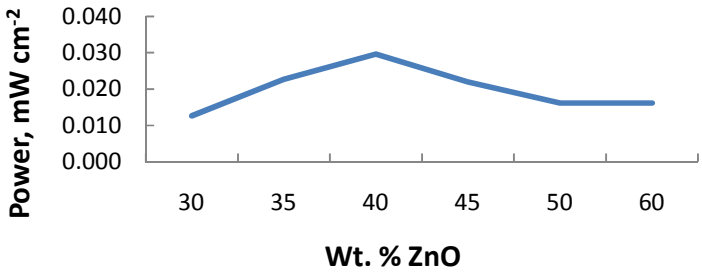

(c)

Figure 9. The variations of (a) voltage, (b) current, and (c) power with the amount of ZnO in the active layer. It is observed that current and voltage tend to change in opposite directions as the ZnO content changes, and that the variation is approximately exponential.

Even though thinner layers limit absorption, it is often necessary to use them with cells of this material composition due to issues with charge transport. Particularly, over the longer distance of a thicker active layer, it is more difficult to maintain continuous charge transport pathways that reach the electrodes. The thicker active layers in this project, however, yielded a current that was on the same order of magnitude as those found in the literature. This finding suggests that it is possible to achieve higher levels of performance by combining the greater absorption found by increasing the amount of absorbing material with the efficient charge transport of a thinner layer.

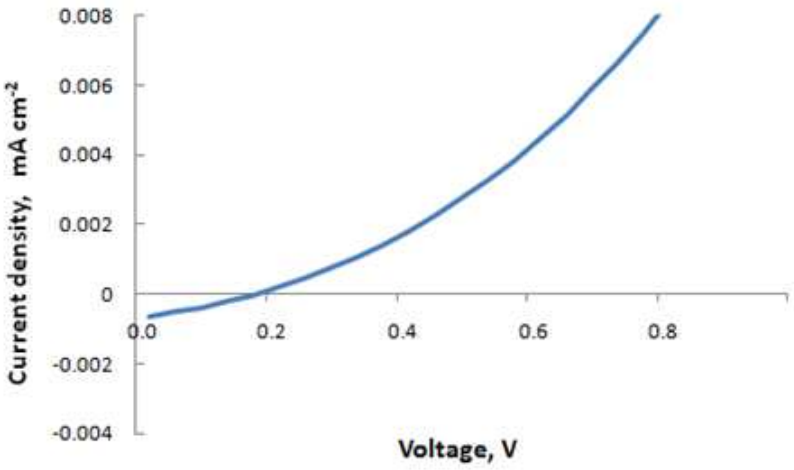

Figure 10. The current-voltage, or J-V, profile of the best performing cell.

3.7 Morphology, performance, and prospects for the future

The Janssen research group [50] of the Netherlands recently published a study on how morphology can affect the performance of P3HT:ZnO solar cells. Using electron tomography, they were able to quantify the spherical contact distance between P3HT and ZnO and the ZnO percolation pathways used for charge transfer in these cells.

Consistent with the principles presented in this paper, they found that charge generation depended on P3HT:ZnO spherical contact distance. The cells that were best at generating charge had approximately 97 % of the P3HT within a 10 nm shortest distance of a ZnO domain. Changing this figure by just a small amount can have a significant difference. In fact, for cells having only 85 % of the P3HT within that same 10 nm shortest distance of a ZnO domain, the performance drops in half.

They also saw that charge transport depended on the ZnO percolation pathways, but there was not as large of a difference in those pathways among the cells tested. One figure reported was the percentage of ZnO that was part of a pathway that actually reached the aluminum electrode (cathode). As the

thickness of the active layer varied, the percentage of ZnO connected to such a pathway varied little.

These results can help us by providing a framework to understand the current work. We see two competing effects: voltage varies inversely with increasing ZnO content, while current varies directly with increasing ZnO content. In light of the study in the literature [50], we know that current depends on the intimacy of mixing of P3HT and ZnO. As the ZnO content increases, there is a larger fraction of P3HT that is close enough to a ZnO domain for charge separation to occur. We see an exponential increase of current with ZnO content in the range tested, and this combined with the data of Oosterhout *et. al.* [50] can allow us to more precisely quantify the intimacy of mixing and how it affects performance.

Additional ZnO also increases the amount and size of percolation pathways, which further improves charge transport. The reason that the increase in current does not continue to occur with additional ZnO content past a certain point is most probably due to competing absorption factors: with greater amounts of ZnO, there is less light-absorbing P3HT. Hence the need to

find an optimal ratio, which is what this project set out to determine quantitatively.

The observed variation of voltage is most likely due to morphological changes as well. Voltage depends on the position of the polymer's energy bands, and these bands can change based on how the physical structure affects polymer-polymer interactions in space [51].

In addition to looking further at the relevant structures, another exciting avenue for future research comes in the form of new materials. For example, the lower band gap of poly[(4,4-bis(2-ethylhexyl)-cyclopenta-[2, 1-*b*; 3,4-*b'*]dithiophene)-2, 6-diyl-*alt*-2, 1, 3-benzothiadiazole-4, 7-diyl], or PCPDTBT, allows it to be a more effective absorber than P3HT. This narrower band gap is due to PCPDTBT being a copolymer that uses alternating electron-withdrawing and electron-donating components to stabilize the quinoidal form of the polymer, narrowing the band gap. Peet *et. al.* [4] have done some work with this material and believe its incorporation can push the performance of organic solar cells to the 10% efficiency threshold.

At the highest level, the goal of this work is to create solutions that allow PV technologies to be made at a low enough cost to compete with energy from

traditional sources. If organic solar cells are going to become a large part of the future of solar power, work must be continued on all facets of their development. One final important factor in this process is the manufacturing techniques used to make these cells. A potential breakthrough is found in roll-to-roll processing [52], which can sharply improve efficiency and lower the processing costs of organic solar cells.

CHAPTER 4

SIGNIFICANCE AND FUTURE WORK

The major focus of this work was on optimizing the ZnO:P3HT solar cell, from its composition through all processing steps. As an intellectual endeavor, the project furthers understanding of this class of cells. Taken in context with other work discussed in section 3.7, this result is magnified.

This type of solar cell is very promising because the materials and processing steps are less expensive than those of existing photovoltaic technology; the major issue is performance. In its current state this technology's performance is so low that, even with the decreased manufacturing cost, the overall cost per unit of energy is still higher. This project addressed the major barriers to increased performance: optimization of processing variables and material composition.

Some further work is already being done using this material combination as an ordered structure rather than a bulk heterojunction. In that arrangement, the ZnO is formed into a repeating nanostructure and the P3HT deposited into it [16]. In principle, this approach can potentially alleviate the issues with charge generation by ensuring that donor-acceptor interfaces occur within an

exciton diffusion length of where the photon is absorbed. This process, however, adds cost into the manufacturing process. It remains to be seen whether the performance can be improved enough to warrant that extra effort.

If it can be further optimized, the bulk heterojunction approach may still prove to be the best route forward. The key to an effective bulk heterojunction is intimacy of mixing and unobstructed pathways to the electrodes. Some new methods of making bulk heterojunctions *in situ*, or mixing the precursors during spin coating, appear promising and seem to warrant further investigation.

REFERENCES

1. U.S. Energy Information Administration, *International Energy Outlook (IEO) 2010*, [online] available: http://www.eia.doe.gov/oiaf/ieo/ 25 May 2010, accessed 24 June 2010

2. Würfel, P, *Physics of Solar Cells: From Basic Principles to Advanced Concepts,* 2009, Wiley VCH, Weinheim, Germany

3. Nelson, J, *The Physics of Solar Cells: Properties of Semiconducting Materials,* 2003, Imperial College Press, London, England

4. Peet, J.; Heeger, A.J.; Bazan, G.C., "Plastic" Solar Cells: Self-Assembly of Bulk Heterojunction Nanomaterials by Spontaneous Phase Separation. *Accounts of Chemical Research*, **2009**, 42, 1700-1708

5. U.S. Department of Energy - Solar Energies Technology Program, *Multi-Year Program Plan 2008-2012,* [online] available: http://www1.eere.energy.gov/solar/pdfs/solar_program_mypp_2008-2012.pdf 15 April 2008, accessed 21 June 2010

6. Dennler, G.; Brabec, C.J., *Socio-Economic Impact of Low-Cost PV Technologies* IN: Brabec, C.; Dyakonov, V.; Scherf, U. [Eds.], *Organic Photovoltaics: Materials, Device Physics, and Manufacturing Technologies*, 2008, Wiley VCH, Weinheim, Germany, pp 531-565

7. Photon Magazine, **2005** (as quoted in ref 6.)

8. The Royal Swedish Academy of Sciences, Press Release, October 10, **2000**

9. Yu , G.; Gao, J.; Hummelen, J.C.; Wudl, F.; Heeger, A.J., Polymer Photovoltaic Cells: Enhanced Efficiencies via a Network of Internal Donor-Acceptor Heterojunctions, Science, **1995**, 270, 1789 – 1791

10. Ewbank, P.C.; Laird, D.; McCullough, R.D., *Regioregular Polythiophene Solar Cells: Material Properties and Performance* IN: Brabec, C.; Dyakonov, V.; Scherf, U. [Eds.], *Organic Photovoltaics: Materials, Device Physics, and*

Manufacturing Technologies, 2008, Wiley VCH, Weinheim, Germany, pp 3-55

11. Brown, P.J.; Thomas, D.S.; Kohler, A.; Wilson, J.S.; Kim, J.S.; Ramsdale, C.M.; Sirringhaus, H.; Friend, R.H., Effect of interchain interactions on the absorption and emission poly(3-hexylthiophene). *Phys. Rev. B*, **2003**, 67, 064203-1 – 064203-16

12. Rieke Materials Online Catalog. P3HT products. [online] available: http://riekemetals.thomasnet.com/viewitems/cialty-conducting-polymers-product-numbers-4000-s-/poly-3-hexylthiophene-2-5-diyl-p3ht accessed 12 July 2010

13. Kline, R.J.; McGehee, M.D., Morphology and charge transport in conjugated polymer. *Polymer Review*, **2006**, 46, 27-45

14. Beek, W. J. E.; Wienk, M. M.; Janssen, R. A. J., Efficient hybrid solar cells from ZnO nanoparticles and a conjugated polymer. *Advanced Materials* **2004**, 16, 1009-1013

15. Beek, W. J. E.; Wienk, M. M.; Janssen, R. A. J., Hybrid polymer solar cells based on zinc oxide. *Journal of Materials Chemistry,* **2005**, **15**, 2985-2988

16. Ravirajan, P.; Peiro, A.M.; Nazeeruddin, M.K.; Graetzel, M.; Bradley, D.D.C.; Durrant, J.R.; Nelson, J., Hybrid Polymer/Zinc Oxide Photovoltaic Devices with Vertically Oriented ZnO Nanorods and an Amphiphilic Molecular Interface Layer. *Journal of Physical Chemistry B*, **2006**, 110, 7635–7639

17. Huynh, W. U.; Dittmer, J.J.; Alivisatos, A.P., Hybrid Nanorod-Polymer Solar Cells. *Science,* **2002** 295, pp. 2425

18. Kwong, C.Y.; Djurisic, A. B.; Chui, P.C.; Cheng, K. W.; Chan, W. K., Influence of solvent on film morphology and device performance of poly(3-hexylthiophene):TiO_2 nanocomposite solar cells. *Chem Phys. Lett,* **2004,** 384, 372-375

19. Cho, N.; Choudhury, K.R.; Thapa, R.B.; Sahoo, Y.; Ohulchanskyy, T.; Cartwright, A.N.; Lee, K.S.; Prasad, P.N., Efficient Photodetection at IR

Wavelengths by Incorporation of PbSe–Carbon-Nanotube Conjugates in a Polymeric Nanocomposite, *Advanced Materials* **2007**, 19, 232–236

20. Nairn, J. J.; Shapiro, P. J.;Twamley, B; Pounds, T.; Wandruszka, R.V.; Fletcher, T. R.; Williams, M.; Wang, C.; Norton, M.G., Preparation of Ultrafine Chalcopyrite Nanoparticles via the Photochemical Decomposition of Molecular Single-Source Precursors. *Nano Letters* **2006**, 6, 1218-1223

21. Peumans, P.; Uchida, S.; Forrest, S.R., Efficient bulk heterojunction photovoltaic cells using small-molecular-weight organic thin films. *Nature,* **2003*,*** 425, 158-162

22. Xue, J.; Uchida, S.; Rand, B.P.; Forrest, S.R., Asymmetric tandem organic photovoltaic cells with hybrid planar-mixed molecular heterojunctions. *Appl. Phys. Lett.*, **2004**, 85, 5757-5759

23. Yang, F.; Shtein, M.; Forrest, S.R., Controlled Growth of a Molecular Bulk Heterojunction Photovoltaic Cell. *Nature Materials*, **2005**, 4, 37-41

24. Drechsel, J.; Männig, B.; Kozlowski, F.; Gebeyehu, D.; Werner, A.; Koch, M.; Leo, K.; Pfeiffer, M., High efficiency organic solar cells based on single or multiple PIN structures. *Thin Solid Films,* **2004**, 451-452, 515-517

25. Greenham, N.C., *Hybrid Polymer/Nanocrystal Photovoltaic Devices* IN: Brabec, C.; Dyakonov, V.; Scherf, U. [Eds.], *Organic Photovoltaics: Materials, Device Physics, and Manufacturing Technologies*, 2008, Wiley VCH, Weinheim, Germany, pp 179-210

26. Barker, J.A.; Ramsdale, C.M.; Greenham, N.C., Modeling the current-voltage characteristics of bilayer polymer photovoltaic devices, *Physical Review B: Condensed Matter*, **2002**, 67, 075205 – 075205-9

27. Kroeze, J.E.; Savenije, T.J.; Vermeulen, M.J.W.; Warman, J.M., Contactless Determination of the Photoconductivity Action Spectrum, Exciton Diffusion Length, and Charge Separation Efficiency in Polythiophene-Sensitized TiO2 Bilayers. *Journal of Physical Chemistry B*, **2003**, 107, 7696-7705

28. Beek, W. J. E.; Wienk, M. M.; Kemerink, M.; Yang, X.; Janssen, R. A. J., Hybrid zinc oxide conjugated polymer bulk heterojunction solar cells. *J. Phys. Chem. B* **2005**, 109, 9505-9516

29. Carter, S.A.; Angelopoulos, M.; Karg, S.; Brock, P.J.; Scott, J.C., Polymeric anodes for improved polymer light-emitting diode performance. *Applied Physics Letters*, **1997**, 70, 2067-2069.

30. Elschner, A.; Bruder, F.; Heuer, H.W.; Jonas, F.; Karback, A.; Kirchmeyer, S.; Thurm, S., PEDT/PSS for efficient hole-injection in hybrid organic light-emitting diodes. *Synthetic Metals*, **2000**, 111, 139-143

31. Kugler, Th.; Salaneck, W.R.; Rost, H.; Holmes, A.B., Polymer band alignment at the interface with indium tin oxide: consequences for light emitting devices, *Chemical Physics Letters*, **1999**, 310, 391-396

32. Liu, Y.; Summers, M.A.; Edder, C.; Fréchet, J.M.J.; McGehee, M.D., Using Resonance Energy Transfer to Improve Exciton Harvesting in Organic-Inorganic Hybrid Photovoltaic Cells. *Advanced Materials*, **2005**, 17, 2960-2964

33. Hagfeldt, A.; Grätzel, M., Light-Induced Redox Reactions in Nanocrystalline Systems. *Chemical Reviews*, **1995**, 95, 49-68

34. Sugiyama, K.; Ishii, H.; Ouchi, Y.; Seki, K., Dependence of indium-tin-oxide work function on surface cleaning method as studied by ultraviolet and x-ray photoemission spectroscopies. *Journal of Applied Physics*, **2000**, 87, 295-298.

35. Jonda, C.; Mayer, A.B.R.; Stolz, U.; Elschner, A.; Karbach, A., Surface roughness effects and their influence on the degradation of organic light emitting devices. *Journal of Materials Science*, **2000**, 35, 5645-5651

36. Elschner, A.; Kirchmeyer, S., *PEDOT-type Materials in Organic Solar Cells* IN: Brabec, C.; Dyakonov, V.; Scherf, U. [Eds.], *Organic Photovoltaics: Materials,*

Device Physics, and Manufacturing Technologies, 2008, Wiley VCH, Weinheim, Germany, pp 213-241

37. van Duren, J.K.J.; Loos, J.; Morrissey, F.; Leewis, C.M.; Kivits, K.P.H.; van Ijzendoorn, L.J.; Rispens, M.T.; Hummelen, J.C.; Janssen, R.A.J., *In-situ* compositional and structural analysis of plastic solar cells. *Advanced Functional Materials*, **2002**, 12, 665-669.

38. Yamamoto, T.; Honda, Y.; Sata, T.; Kokubo, H., Electrochemical behavior of poly(3-hexylthiophene): controlling factors of electric current in electdrochemical oxidation of poly(3-hexylthiophene)s in a solution. *Polymer*, **2004**, 45, 1735-1738

39. Kim, D.H.; Jang, y.; Park, Y.D.; Cho, K., Controlled one-dimensional nanostructures in poly(3-hexylthiophene) thin film for high-performance organic field-effect transistors. *J Phys. Chem. B,* **2006,** 110, 15763-15768

40. Chang, C.C.; Pai, C.L.; Chen, W.C.; Jenekhe, S.A., Spin coating of conjugated polymers for electronic and optoelectronic applications. *Thin Solid Films,* **2005,** 479, 254-260

41. DeLongchamp, D.M.; Vogel, B.M.; Jung, Y.; Gurau, M.C.; Richter, C.A.; Kirillov, O.A.; Obrzut, J.; Fischer, D.A.; Sambasivan, S.; Richter, L.J.; Lin, E.K., Variations in semiconducting polymer microstructure and hole mobility with spin-coating speed. *Chemistry of Materials,* **2005**, 17, 5610-5612

42. Huynh, W. U.; Dittmer, J. J.; Libby, W. C.; Whiting, G. L.; Alivisatos, A. P., Controlling the morphology of nanocrystal-polymer composites for solar cells. *Advanced Functional Materials* **2003,** 13, (1), 73-79.

43. Shrotriya, V; Li, G.; Yao, Y.; Moriarty, T.; Emery, K.; Yang, Y., Accurate measurement and characterization of organic solar cells. *Advanced Functional Materials,* **2006**, 16, 2016-2023

44. ASTM Standard E 772-05, Standard Terminology Relating to Solar Energy Conversion, American Society for Testing and Materials, West Conshocken, PA

45. Meulenkamp, E. A., Synthesis and growth of ZnO nanoparticles. *J Phys. Chem. B,* **1998,** 102, 5566-5572

46. Spanhel, L.; Anderson, M., Semiconductor clusters in the sol-gel process: quantized aggregation, gelation, and crystal growth in concentrated zinc oxide colloids. *Journal of the American Chemical Society,* **1991**, 113, 2826-2833

47. Roy, B.; Karmakar, B.; Bahadur, J.; Mazumder, S.; Sen, D.; Pal, M., Structural characterization of manganese-substituted nanocrystalline zinc oxide using small-angle neutron scattering and high-resolution transmission electron microscopy. *Journal of Applied Crystallography*, **2009**, 42, 1085-1091

48. Kroon, J.M.; Wienk, M.M.; Verhees, W.J.H.; Hummelen, J.C., Accurate efficiency determination and stability studies of conjugated polymer/fullerene solar cells. *Thin Solid Films,* **2002**, 403, 223-228

49. Wang, M.; Wang, X., P3HT/ZnO bulk-heterojunction solar cell sensitized by a perylene derivative. *Solar Energy Materials and Solar Cells*, 92, **2008**, 766

50. Oosterhout, S.D.; Wienk, M.M.; van Bavel, S.S; Thiedmann, R.; Koster, L.J.A.; Gilot, J; Loos, J.; Schmidt, V.; Janssen, R.A.J., The effect of three-dimensional morphology on the efficiency of hybrid polymer solar cells. *Nature Materials*, **2009,** 8, 818-824

51. Beek, W. J. E.; Wienk, M. M.; Janssen, R. A. J., *Metal Oxide-Polymer Bulk Heterojunction Solar Cells* IN: Brabec, C.; Dyakonov, V.; Scherf, U. [Eds.], *Organic Photovoltaics: Materials, Device Physics, and Manufacturing Technologies*, 2008, Wiley VCH, Weinheim, Germany, pp 357-397.

52. Krebs, F.C.; Gevorgyan, S.A.; Alstrup, J., A roll-to-roll process to flexible polymer solar cells: model studies, manufacture, and operational stability studies. *Journal of Materials Chemistry*, **2009**, 19, 5442-5451

53. Rispens, M.T.; Meetsma, A.; Rittberger, R.; Brabec, C.J.; Sariciftci, N.S.; Hummelen, J.C., Influence of the solvent on the crystal structure of PCBM and the efficiency of MDMO-PPV:PCBM “plastic” solar cells. *Chemical Communications*, **2003**, 2116-2118

54. Loos, J.; van Bavel, S.; Yang, X.; *Morphology of Bulk Heterojunction Solar Cells* IN: Brabec, C.; Dyakonov, V.; Scherf, U. [Eds.], *Organic Photovoltaics: Materials, Device Physics, and Manufacturing Technologies*, 2008, Wiley VCH, Weinheim, Germany, pp 299-325

55. Genley, D.S.; Bright, C., Transparent conducting oxides. *MRS Bulletin*, **2000**, 25, 15-21

VITA

Garrett Morgan Salpeter was born in Oak Brook, Illinois. After graduation from Benet Academy in Lisle, Illinois, he attended Middelebury College, Middlebury, Vermont, where he was awarded a Bachelor of Arts degree in Physics in May, 2008. Upon graduation, he entered the Graduate School at the University of Texas at Austin in August, 2008.

Email: garrett@garrettsalpeter.com

This thesis was typed by the author.